

Unraveling Structure and Device Operation of Organic Permeable Base Transistors

Ghader Darbandy,* Felix Dollinger,* Petr Formánek, René Hübner, Stefan Resch, Christian Roemer, Axel Fischer, Karl Leo, Alexander Kloes, and Hans Kleemann

Organic permeable base transistors (OPBTs) are of great interest for flexible electronic circuits, as they offer very large on-current density and a record-high transition frequency. They rely on a vertical device architecture with current transport through native pinholes in a central base electrode. This study investigates the impact of pinhole density and pinhole diameter on the DC device performance in OPBTs based on experimental data and TCAD simulation results. A pinhole density of $N_{\text{pin}} = 54 \mu\text{m}^{-2}$ and pinhole diameters around $L_{\text{pin}} = 15 \text{ nm}$ are found in the devices. Simulations show that a variation of pinhole diameter and density around these numbers has only a minor impact on the DC device characteristics. A variation of the pinhole diameter and density by up to 100% lead to a deviation of less than 4% in threshold voltage, on/off current ratio, and sub-threshold slope. Hence, the fabrication of OPBTs with reliable device characteristics is possible regardless of statistical deviations in thin film formation.

1. Introduction

Organic thin film transistors have great potential in flexible electronic applications like electronic displays^[1] as well as in low-cost devices like RFID tags.^[2] The performance of organic transistors has greatly improved in recent years due to optimization

in charge carrier mobility,^[3,4] contact resistance,^[5,6] device design, and fabrication methods.^[7–9] To further improve the performance of organic transistors, in particular with regard to high-frequency operation, researchers developed various approaches for vertical transistors,^[10] which offer exceptional device operation frequency due to an ultra-short channel length. One special vertical organic transistor, the Organic Permeable Base Transistor (OPBT), is currently the highest-frequency organic transistor with a transition frequency of up to 40 MHz.^[11] It is of great interest, because it makes use of comparably simple thin film processes to create transistor structures with extremely small dimensions.^[12,13] At the same time, it can also be employed

as a four-terminal device for built-in logical operations.^[14] Identical or similarly structured transistor devices are also published under the names Metal-Base Organic Transistor (MBOT)^[15] or Space-Charge Limited Transistor (SCLT).^[16,17] The formation of a native oxide layer and of nano-sized pinholes in the thin metallic base electrode are utilized, providing very small structure sizes to define the transistor channel. The short channel length leads to large current densities^[18] and, consequently, high transition frequencies. Additionally, the limiting influence of contact resistance is reduced in OPBTs, because of their ability to inject current over the entire device area.^[19]

The central base electrode in an OPBT device is permeable to electrons via nano-sized intrinsically grown pinholes in the metal film,^[20] allowing for current transport through the device, as indicated in **Figure 1**. A voltage applied between base and emitter is capable of modulating the current between emitter and collector over many orders of magnitude. The pinholes in the metallic base layer appear due to strain in this layer during the oxidation. This intrinsic and self-limiting process though is expected to show statistical variations in pinhole size and density which might affect the transistor's performance. In this work, we evaluate the size and density of these pinholes by experiment and evaluate the impact of variations on the device performance based on TCAD (Technology Computer Aided Design) simulations.

Dr. G. Darbandy, S. Resch, C. Roemer, Prof. A. Kloes
NanoP

TH Mittelhessen University of Applied Sciences
Giessen 35390, Germany
E-mail: Ghader.Darbandy@ei.thm.de

Dr. F. Dollinger, Dr. A. Fischer, Dr. H. Kleemann, Prof. K. Leo
Dresden Integrated Center for Applied Physics and Photonic Materials (IAPP) and Institute for Applied Physics
Technische Universität Dresden
Dresden 01062, Germany
E-mail: felix.dollinger@tu-dresden.de

Dr. P. Formánek
Leibniz-Institut für Polymerforschung Dresden e.V. (IPF)
Dresden 01069, Germany

Dr. R. Hübner
Institute of Ion Beam Physics and Materials Research
Helmholtz-Zentrum Dresden-Rossendorf
Dresden 01328, Germany

 The ORCID identification number(s) for the author(s) of this article can be found under <https://doi.org/10.1002/aelm.202000230>.

© 2020 The Authors. Published by WILEY-VCH Verlag GmbH & Co. KGaA, Weinheim. This is an open access article under the terms of the Creative Commons Attribution License, which permits use, distribution and reproduction in any medium, provided the original work is properly cited.

DOI: 10.1002/aelm.202000230

2. Device Fabrication and TCAD Simulation

Organic Permeable Base Transistors are fabricated by consecutive vacuum evaporation of the electrode and semiconductor

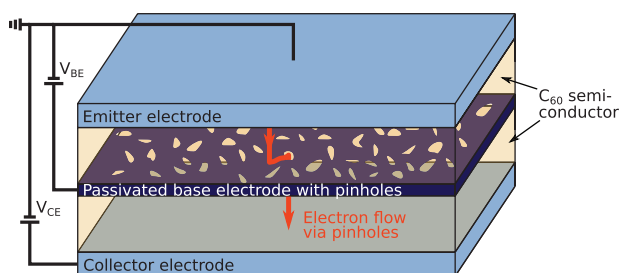


Figure 1. Device stack of an OPBT. The central base electrode is permeable to electrons. The device current flows between emitter and collector, while the base layer is passivated by an oxide layer. The device current can be modulated by the base-emitter voltage V_{BE} .

layers. A passivating oxide film of Al_2O_3 around the aluminum base electrode is formed by native oxidation in air or with an electrochemically controlled process.^[21–23] The devices consist of an organic semiconductor layer sandwiched between the collector and emitter electrodes and the thin base electrode, which is permeable to electrons, in the center. Typical layer thicknesses are 100 nm for the collector and emitter electrodes and the semiconductor layers and 15 nm for the base electrode. Electrical DC measurements on fabricated OPBTs with C_{60} as organic semiconductor (OSC) have been taken as a reference for the Sentaurus TCAD simulation setup.^[24]

For investigation of the properties of the base layer in a transmission electron microscope (TEM), a base-only device is prepared: A TEM-grid is vacuum-coated with a 50 nm thick C_{60} layer to provide the same surface and morphology as in an OPBT device. Then, a 15 nm film of aluminum is deposited and exposed to ambient air in the dark for 15 min to ensure native oxidation of the metal. This oxidation process is also employed for all devices used for electrical testing. High-angle annular dark-field scanning transmission electron microscopy and spectrum imaging based on energy-dispersive X-ray spectroscopy (HAADF-STEM and EDXS) are conducted with a Talos F200X (Thermo Fischer Scientific/FEI, USA) operated at 200 kV and equipped with a Super-X EDX detector. The latter provides detailed element maps (C, O, Al) of the base layer. The pinholes are manifested by decreased X-ray counts in the aluminum map.

For TCAD simulations, the device is modeled as illustrated in **Figure 2a**. The data shown in **Figure 2b** reveals a quite reasonable agreement of the DC characteristics between simulations (solid lines) and the measurements (symbols) for the parameter values denoted in **Table 1** (device dimensions for **Figure 2b** are $W = 250 \mu\text{m}$ and $L_E = 250 \mu\text{m}$). In order to remove an initial hysteresis in the device from the measurement, the voltage is swept up and down for several times.^[25] A Poole–Frenkel mobility model with a square-root dependence on the electric field, as represented by Equation (1) and a Gaussian density of state (DOS), as in Equation (2), are used with the default values.^[24]

$$\mu(F) = \mu_0 \exp\left(-\frac{E_0}{kT}\right) \exp\left(\sqrt{F}\left(\frac{\beta}{T} - \gamma\right)\right) \quad (1)$$

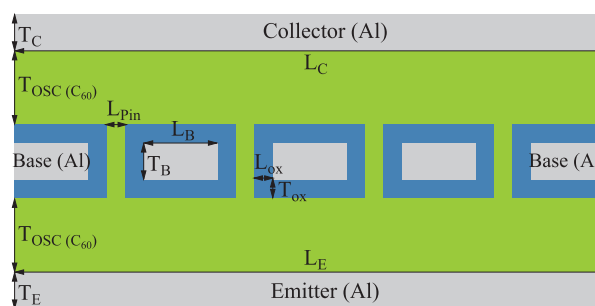
where μ_0 is the low-field mobility, E_0 is the effective activation energy, k is the Boltzmann constant, T is the temperature, β and γ are the Poole–Frenkel coefficients, and F is the applied electric field. The Gaussian DOS is described by

$$g(E) = \frac{N_c}{\sqrt{2\pi}\sigma_{DOS}} \exp\left(-\frac{(E - E_c)^2}{2\sigma_{DOS}^2}\right) \quad (2)$$

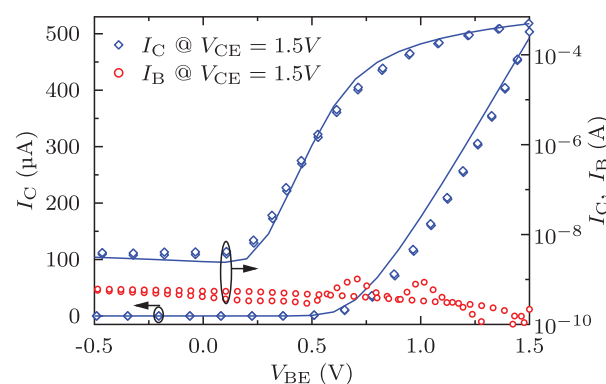
where N_c is the effective density of states, σ_{DOS} is the width of the DOS distribution, and E_c is the energy center.

In the framework of hopping transport, charge carriers are localized on individual molecules due to the weak overlap of intermolecular orbitals and only occasionally hop to other favorable molecular sites. Thus, charges cannot be treated as plane waves, and hence, a quantum confinement due to the pinhole size is not expected.

Furthermore, it should be emphasized that the base leakage current I_B is quite small and negligible compared to the collector current I_C (see **Figure 2b**). Hence, the base leakage current has no influence on the device DC characteristics including the threshold voltage V_{th} , on/off current ratio, sub-threshold slope SS , etc.



(a) OPBT structure used for Sentaurus TCAD simulation



(b) Transfer I_C and Base Leakage Current I_B at $V_{CE} = 1.5\text{V}$

Figure 2. a) Schematic cross-section of the simulated OPBT used for Sentaurus TCAD setup and b) Transfer characteristics I_C (the double symbols indicate forward and backward sweep) from experimental ($W = 250 \mu\text{m}$ and $L_E = 250 \mu\text{m}$) data (symbols) compared with data from TCAD simulation (solid lines) including the base leakage current I_B (circles) for $V_{CE} = 1.5\text{V}$.

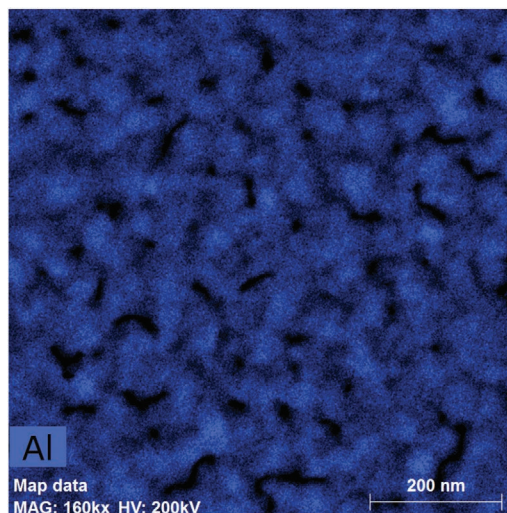
Table 1. Parameters and units used for 3D OPBT TCAD simulation.

Quantity	Value/Unit
Device width W	1 μm
Device length $L_E = L_C$	1 μm
OSC thickness T_{OSC}	100 nm
Oxide thickness $T_{\text{ox}} = L_{\text{ox}}$	5 nm
Pinhole diameter L_{pin}	4 nm
Number of pinholes N_{pin}	50 μm^{-2}
Base/emitter/collector thickness $T_{\text{B/E/C}}$	10 nm
Low field mobility μ_0	3 $\text{cm}^2 \text{Vs}^{-1}$
Effective density of states N_C	1 · 10 ²¹ cm^{-3}
Width of the DOS distribution σ_{DOS}	0.081 eV
Energy center E_c	0.1 eV
Temperature T	300 K
Poole Frenkel coefficient β	3
Poole Frenkel coefficient γ	0

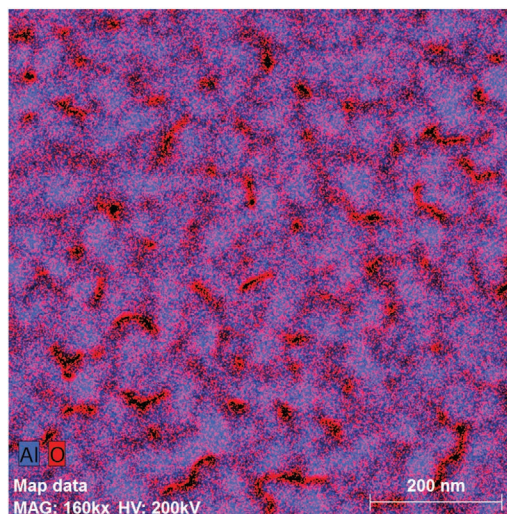
2.1. Pinhole Size Distribution Analyzed by TEM

To analyze the morphology and element distribution of the Al base layer as well as to deduce the pinhole size distribution, EDXS-based chemical mapping was performed in scanning TEM mode. The distribution of aluminum is shown in Figure 3a. The 15 nm thin film is percolated, providing a conductive electrode that can distribute an applied base potential across the entire device. Between the conductive paths, voids are visible where no aluminum is present. These voids are pinholes in the film and will be filled by C_{60} , hence allowing for vertical electron transport through the device. By adding the information about the distribution of oxygen atoms in the layer, Figure 3b is obtained. It shows that the base electrode layer is evenly oxidized. At the rims of the pinholes, a stronger oxygen signal is visible, representing the oxidation of the vertical sidewalls of each pinhole. Since the thickness of the sidewall-oxide is uniform throughout the sample, every void in the aluminum film that is above a certain size has a remaining opening in its center. The structure is analyzed using a grey-scale threshold value to identify voids. Noticeable voids of at least 25 nm^2 are considered as pinholes. The density of the so-defined pinholes is found to be 54 per μm^2 . Their size distribution can be seen in Figure 4. Typical dimensions of the mostly elongated pinholes are between 5 and 25 nm.

Based on these findings and the insight that thin-film formation is always a statistical process, the questions arise, which pinhole density and dimension would be ideal for the OPBT and how deviations in the microstructure will influence the device characteristics. It has previously been shown that the pinhole size and density is not limiting the maximum current level in an OPBT, but only determines the device behavior at low base potential.^[12] Nevertheless, it is of interest to investigate how fluctuations in the pinhole formation will influence the device performance and hence affect the reproducibility in a potential large-scale OPBT production. In the following, answers to these questions will be given based on TCAD simulations.



(a)



(b)

Figure 3. Energy-dispersive X-ray spectroscopy (EDXS) based element maps of the base layer showing well-passivated pinholes in the metallic film. a) Aluminum distribution. b) Superimposed Al and O distributions, proving that the sample is uniformly oxidized and that the pinholes are free of both elements.

2.2. Pinhole Diameter L_{pin}

Using TCAD simulations, we discuss the effect of a variation of the pinhole diameter L_{pin} on the device currents, threshold voltage, and subthreshold slope. We vary L_{pin} from 2 to 100 nm in order to cover the entire range of what is experimentally observed.

Figure 5 shows the simulated transfer characteristics of an OPBT for different diameters of the pinholes L_{pin} at $V_{\text{CE}} = 1.5 \text{ V}$. The on-current is increasing slightly with the diameter of the pinholes, while the off-current remains almost constant up to $L_{\text{pin}} = 50 \text{ nm}$ and drastically increases with $L_{\text{pin}} = 100 \text{ nm}$.

The reasons for an increased off-current for large L_{pin} are the reduced base control over the channel and increased short-channel effects.

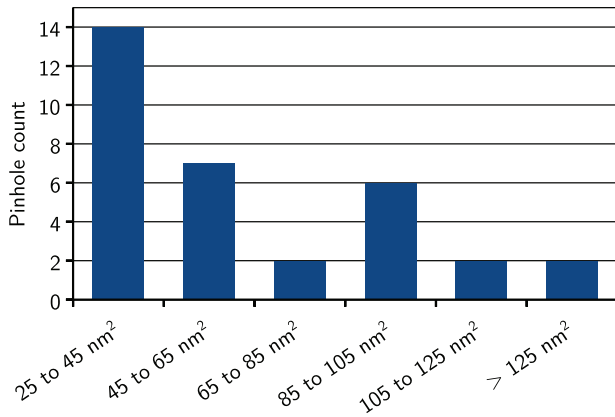


Figure 4. Histogram of pinhole size distribution.

Figure 6 shows the on- ($V_{BE} = 1.5$ V) and off- ($V_{BE} = 0$ V) current in more detail as a function of the pinhole diameter at $V_{CE} = 1.5$ V. As can be seen in Figure 6b, the on-current increases from 500 up to 510 μ A (2%) for a pinhole diameter variation of 100% from 6 to 12 nm. Therefore, the pinhole diameter is not the main limiting factor of the OPBT current I_{CE} . This is in agreement with earlier findings that show the total device current in the on-state to reach a space-charge-limited current in the OSC.^[18] A very small deviation of the threshold voltage (extracted as the intersection of the tangent at the maximum conductance) and subthreshold slope is shown as a function of pinhole diameter in Figure 6c. The threshold voltage is about $V_{th} = 0.72$ V for a pinhole diameter of $L_{Pin} = 6$ nm and $V_{th} = 0.70$ V for $L_{Pin} = 12$ nm. This means a shift in the threshold voltage of about 3% is expected with an increase of 100% in pinhole diameter. The subthreshold slope is about $SS = 115$ mV dec^{-1} for a pinhole diameter of $L_{Pin} = 6$ nm and $SS = 126$ mV dec^{-1} for $L_{Pin} = 12$ nm, resulting in a slope degradation of up to 10%.

Figure 7 displays the charge and current density profiles of the OPBT with one single pinhole at $V_{CE} = V_{BE} = 3$ V. The whole device current I_C has to pass through the pinhole, thus there is a high current density in this opening and the opening size might be a current-limiting factor. The charge and current

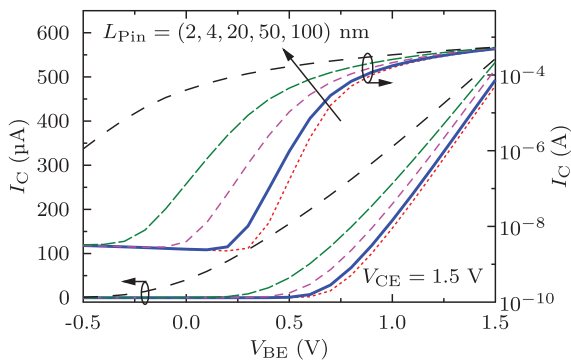
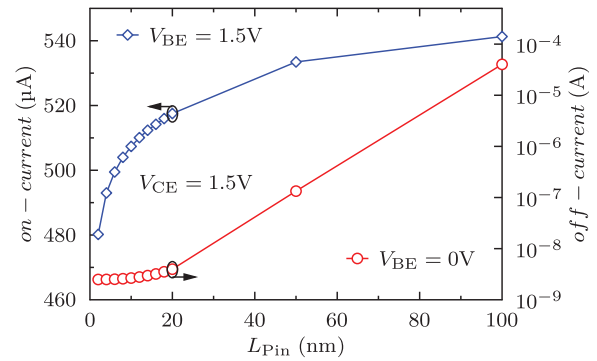
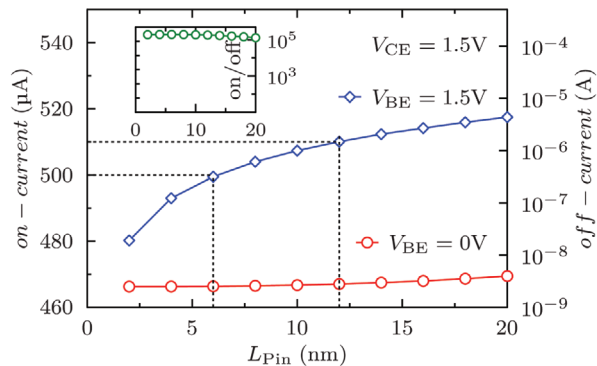


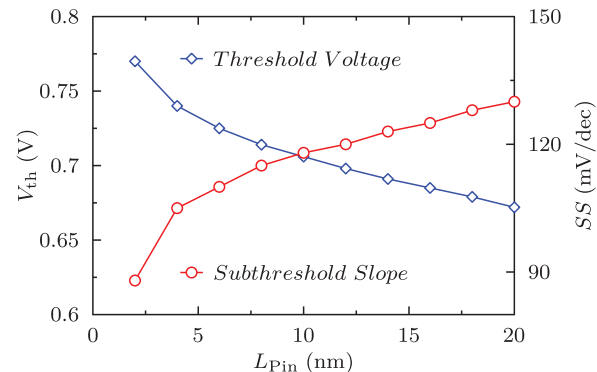
Figure 5. Simulated transfer characteristics of an OPBT for different pinhole diameter L_{Pin} (see legend). Bias information: $V_{CE} = 1.5$ V, $N_{Pin} = 50 \mu m^{-2}$, device width $W = 250 \mu m$ and length $L_E = 250 \mu m$.



(a) Simulated on- and off-current



(b) Simulated on- and off-current (zoom in)



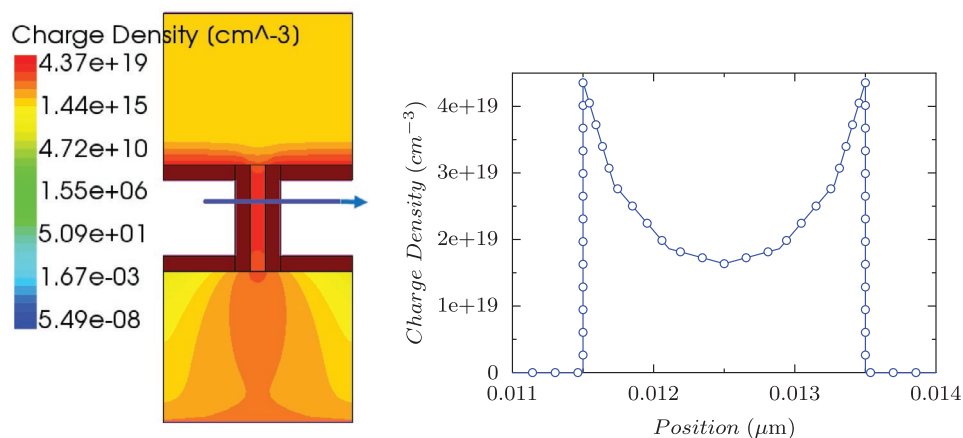
(c) Simulated V_{th} and SS

Figure 6. Simulated on- ($V_{BE} = 1.5$ V) and off- ($V_{BE} = 0$ V) current as a function of the pinhole diameter a) up to $L_{Pin} = 100$ nm, b) zoom in up to $L_{Pin} = 20$ nm at $V_{CE} = 1.5$ V (inset shows I_{on}/I_{off}), and c) threshold voltage (V_{th}) and subthreshold slope (SS).

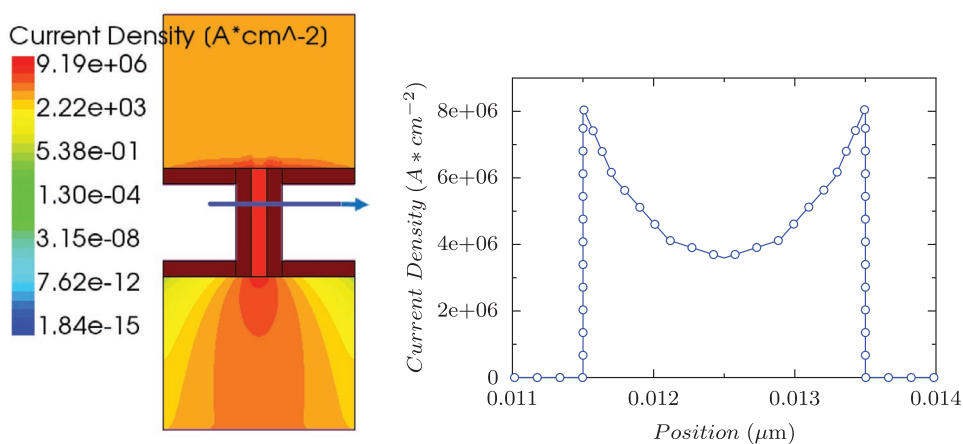
densities have their maximum at the semiconductor/oxide interface due to the electrostatic and applied base bias V_{BE} .

2.3. Number of Pinholes N_{Pin}

The influence of a variation of the pinhole density from the targeted value of about $50 \mu m^{-2}$ in the fabricated real devices has been investigated to show the current flow deviation with



(a) Charge density profile



(b) Current density profile

Figure 7. a) Charge carrier density and b) current density profile through the pinhole (see the cutline) at $V_{CE} = V_{BE} = 3$ V.

the number of pinholes per μm^2 . The deviation of DC characteristics (on- and off-current, threshold voltage V_{th} , and sub-threshold slope SS) of OPBTs is shown as a function of the pinhole density in **Figure 8**.

Figure 8a shows that the on-current is increasing with the number of pinholes per μm^2 . It is, however, not linearly dependent on the number of pinholes. The current I_C increases slightly with an additional pinhole. Hence, the on-current ($V_{BE} = 1.5$ V) must saturate at a certain number of pinholes per μm^2 .

Figure 8b shows that a variation of pinhole density from the target value of $50 \mu\text{m}^{-2}$ up to $100 \mu\text{m}^{-2}$ (an increase of 100%) has a negligible (almost 2%) impact on the device on-current. Thus, the OPBTs on-current does not significantly depend on the number of pinholes within a large range. The off-current I_{OFF} ($V_{BE} = 0$ V) remains almost constant for different pinhole densities (see **Figure 8b**), and also the impact on the threshold voltage and subthreshold slope is negligible (**Figure 8c**).

Therefore, a very small deviation in the DC characteristics of OPBTs is expected with the variation of the number of pinholes per μm^2 .

3. Conclusion

In this work, it has been shown that even significant variations of the pinhole diameter and pinhole density from the targeted values have a negligible impact on OPBT DC characteristics. For a wide parameter range, the OPBT performance is not limited by the pinholes, but rather by the vertical current transport in the OSC.

Stable and reproducible DC characteristics can be expected and achieved regardless of statistical variations in the fabrication of the base layer in OPBTs in terms of a deviation of pinhole diameter and density.

Acknowledgements

G.D. and F.D. contributed equally to this work. This project was funded by the German Research Foundation (DFG) under the grants KL 1042/9-2 and LE 747/52-2 (SPP FFLexCom) and by the European Community's Seventh Framework Programme under Grant Agreement

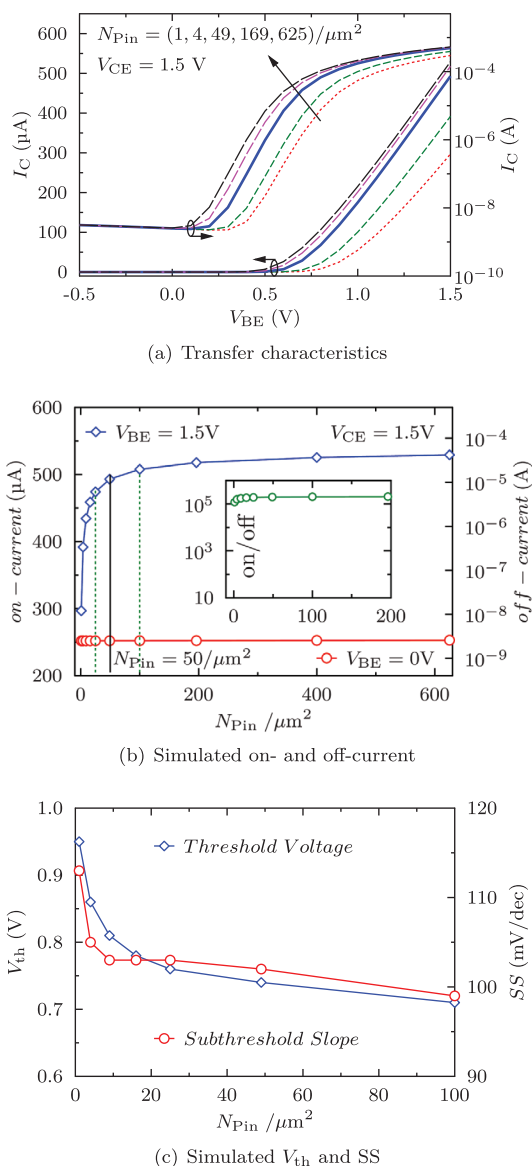


Figure 8. a) Simulated transfer characteristics with $L_{Pin} = 4$ nm and different number of pinholes N_{Pin} (see legend), b) Simulated on ($V_{BE} = 1.5$ V) and off ($V_{BE} = 0$ V) current as a function of pinhole number (inset shows I_{on}/I_{off}), and (c) Simulated V_{th} and SS .

No. FP7-267995 (NUDEV). This work was supported in part by the German Research Foundation (DFG) within the Cluster of Excellence Center for Advancing Electronics Dresden (cfaed) and the DFG project HEFOS (Grant No. FI 2449/1-1). Furthermore, the use of HZDR Ion Beam Center TEM facilities and the funding of TEM Talos by the German Federal Ministry of Education and Research (BMBF; grant No. 03SF0451) in the frame-work of HEMCP are acknowledged. The authors thank Tobias Günther and Andreas Wendel of IAPP for sample preparation.

Conflict of Interest

The authors declare no conflict of interest.

Keywords

organic permeable base transistors, organic electronics, technology computer-aided design simulation

Received: March 3, 2020

Revised: May 11, 2020

Published online: June 11, 2020

- [1] M. Furno, H. Kleemann, G. Schwartz, J. Blochwitz-Nimoth, *SID Symposium Digest of Technical Papers* **2015**, 46, 597.
- [2] A. Yamamura, H. Matsui, M. Uno, N. Isahaya, Y. Tanaka, M. Kudo, M. Ito, C. Mitsui, T. Okamoto, J. Takeya, *Adv. Electron. Mater.* **2017**, 3, 1600456.
- [3] M. Nikolka, I. Nasrallah, B. Rose, M. K. Ravva, K. Broch, A. Sadhanala, D. Harkin, J. Charmet, M. Hurhangee, A. Brown, S. Illig, P. Too, J. Jongman, I. McCulloch, J.-L. Bredas, H. Sirringhaus, *Nat. Mater.* **2016**, 16, 356.
- [4] S. Kumagai, M. Nakano, K. Takimiya, J. Takeya, *Org. Electron.* **2018**, 62, 548.
- [5] J. W. Borchert, B. Peng, F. Letzkus, J. N. Burghartz, P. K. L. Chan, K. Zojer, S. Ludwigs, H. Klauk, *Nat. Commun.* **2019**, 10, 1.
- [6] C. Liu, Y. Xu, Y. Y. Noh, *Mater. Today* **2015**, 18, 79.
- [7] K. Fukuda, Y. Takeda, Y. Yoshimura, R. Shiwaku, L. T. Tran, T. Sekine, M. Mizukami, D. Kumaki, S. Tokito, *Nat. Commun.* **2014**, 5, 1.
- [8] P. K. L. Chan, *Adv. Electron. Mater.* **2019**, 1900029.
- [9] M. Höppner, D. Kneppel, H. Kleemann, K. Leo, *Org. Electron.* **2020**, 76, 105357.
- [10] H. Kleemann, K. Krechan, A. Fischer, K. Leo, *Adv. Funct. Mater.* **2020**, 1907113.
- [11] B. Kheradmand-Boroujeni, M. P. Klinger, A. Fischer, H. Kleemann, K. Leo, F. Ellinger, *Sci. Rep.* **2018**, 8.
- [12] F. Kaschura, A. Fischer, M. P. Klinger, D. H. Doan, T. Koprucki, A. Glitzky, D. Kasemann, J. Widmer, K. Leo, *J. Appl. Phys.* **2016**, 120, 094501.
- [13] M. P. Klinger, A. Fischer, F. Kaschura, R. Scholz, B. Lüssem, B. Kheradmand-Boroujeni, F. Ellinger, D. Kasemann, K. Leo, *Adv. Mater.* **2015**, 27, 7734.
- [14] E. Guo, Z. Wu, G. Darbandy, S. Xing, S.-J. Wang, A. Tahn, M. Göbel, A. Kloes, K. Leo, H. Kleemann, *Preprints* **2020**, <https://doi.org/10.20944/preprints202005.0013.v1>.
- [15] G. Giusi, E. Sarnelli, M. Barra, A. Cassinese, G. Scandurra, K. Nakayama, C. Ciofi, *IEEE Trans. Electron Devices* **2017**, 64, 4260.
- [16] H. Fukagawa, Y. Watanabe, K. Kudo, J.-i. Nishida, Y. Yamashita, H. Fujikake, S. Tokito, T. Yamamoto, *AIP Adv.* **2016**, 6.
- [17] K. M. Huang, H. C. Lin, K. Kawashima, I. Osaka, H.-W. Zan, H. F. Meng, K. Takimiya, *Org. Electron.* **2017**, 50, 325.
- [18] M. P. Klinger, A. Fischer, F. Kaschura, J. Widmer, B. Kheradmand-Boroujeni, F. Ellinger, K. Leo, *Sci. Rep.* **2017**, 7, 44713.
- [19] A. Al-Shadeedi, S. Liu, V. Kaphle, C. M. Keum, B. Lüssem, *Adv. Electron. Mater.* **2019**, 5, 1800728.
- [20] K. N. Subedi, A. Al-Shadeedi, B. Lüssem, *Appl. Phys. Lett.* **2019**, 115, 193301.
- [21] F. Dollinger, K. G. Lim, Y. Li, E. Guo, P. Formánek, R. Hübner, A. Fischer, H. Kleemann, K. Leo, *Adv. Mater.* **2019**, 31, 1900917.
- [22] F. Dollinger, H. Iseke, E. Guo, A. Fischer, H. Kleemann, K. Leo, *Adv. Electron. Mater.* **2019**, 5, 1900576.
- [23] S. Liu, R. K. Radha Krishnan, A. Al-Shadeedi, B. Lüssem, *ACS Appl. Electron. Mater.* **2019**, 1, 1756.
- [24] Sentaurus Device User Manual, TCAD, Synopsys, CA, USA, Version June 2018, 2018.
- [25] G. Darbandy, C. Roemer, J. Leise, J. Pruefer, J. W. Borchert, H. Klauk, A. Kloes, presented at 2019 MIXDES-26th Int. Conf. "Mixed Design of Integrated Circuits and Systems", Rzeszów, Poland **2019**, pp. 76–80.